Accepted Manuscript

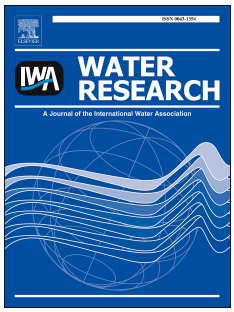

Catalytic hydrodechlorination of triclosan using a new class of anion-exchange-resin supported palladium catalysts

Bing Han, Wen Liu, Jingwen Li, Jin Wang, Dongye Zhao, Rui Xu, Zhang Lin

PII: S0043-1354(17)30327-5

DOI: 10.1016/j.watres.2017.04.059

Reference: WR 12858

To appear in: *Water Research*

Received Date: 12 February 2017

Revised Date: 23 April 2017

Accepted Date: 25 April 2017

Please cite this article as: Han, B., Liu, W., Li, J., Wang, J., Zhao, D., Xu, R., Lin, Z., Catalytic hydrodechlorination of triclosan using a new class of anion-exchange-resin supported palladium catalysts, *Water Research* (2017), doi: 10.1016/j.watres.2017.04.059.

Graphical Abstract

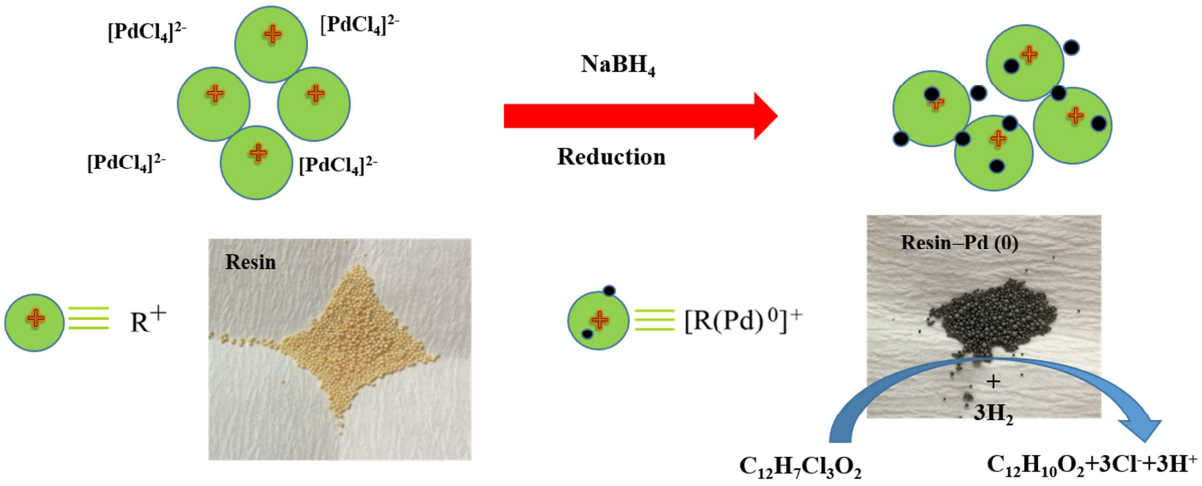

Catalytic Hydrodechlorination of Triclosan Using a New Class of Anion-Exchange-Resin Supported Palladium Catalysts

Bing Han[a], Wen Liu[a], Jingwen Li[a], Jin Wang[a], Dongye Zhao[a,*], Rui Xu[b], Zhang Lin[c]

[a] Environmental Engineering Program, Department of Civil Engineering, Auburn University, Auburn, AL 36849, USA

[b] Department of Chemical Engineering, Auburn University, Auburn, AL 36849, USA

[c] School of Environment and Energy, South China University of Technology, Guangzhou 510006, China

* Corresponding author: Phone: +01 (334) 844 6277; Fax: +01 (334) 844 6290; E-mail: zhaodon@auburn.edu

Abstract

We prepared a new class of anion-exchange-resin supported Pd catalysts for efficient hydrodechlorination of triclosan in water. The catalysts were prepared through an initial ion-exchange uptake of $PdCl_4^{2-}$ and subsequent reduction of Pd(II) to Pd(0) nanoparticles at ambient temperature. Two standard strong-base anion exchange resins (IRA-900 and IRA-958) with different matrices (polystyrene and polyacrylic) were chosen as the supports. SEM and TEM images showed that Pd(0) nanoparticles were evenly attached on the resin surface with a mean size of 3-5 nm. The resin supported Pd catalysts (Pd@IRA-900 and Pd@IRA-958) were able to facilitate rapid and complete hydrodechlorination of triclosan. At a Pd loading of 2.0 wt.%, the observed pseudo first-order rate constant (k_{obs}) was 1.25±0.06 and 1.6±0.1 L/g/min for Pd@IRA-900 and Pd@IRA-958, respectively. The catalysts were more resistant to Cl^- poisoning and natural organic matter fouling than other supported-Pd catalysts. The presence of 10 mM NaCl suppressed the k_{obs} value by 31% and 23% for Pd@IRA-900 and Pd@IRA-958, whereas the presence of humic acid at 30 mg/L as TOC lowered the rates by 28% and 27%, respectively. The better performance of Pd@IRA-958 was attributed to the polymeric matrix properties (i.e., hydrophobicity, pore size, and surface area) as well as Pd particle size. GC/MS analyses indicated that very low concentrations of chlorinated intermediates were detected in the early stage of the hydrodechlorination process, with 2-phenoxyphenol being the main byproducts. The catalysts can be repeatedly used in multiple operations without significant bleeding. The catalysts eliminate the need for calcination in preparing conventional supported catalysts, and the resin supports conveniently facilitate control of Pd loading and material properties.

Keywords: Pharmaceutical and personal care product; Catalysis; Emerging contaminant; Hydrodechlorination; Reductive dechlorination; Supported catalysts

1. Introduction

Triclosan, or 5-chloro-2-(2,4-dichlorophenoxy)phenol, is a broad-spectrum antimicrobial agent. It has been used worldwide as a preservative or an antiseptic agent in many personal care and household products (e.g., toothpaste, soaps, deodorants, shampoos, cosmetics, and plastic additives). Due to the massive consumption, large amounts of triclosan are discharged into wastewater treatment systems and water bodies. The U.S. Geological Survey reported that triclosan was among the seven most frequently detected organic contaminants in 139 streams sampled across 30 states in the U.S. with a median concentration of 0.14 µg/L (Kolpin et al., 2002).

There have been growing concerns about the environmental persistence of triclosan and its health risks to human and aquatic lives. Triclosan is an endocrine disrupting chemical that can cause adverse effects on the thyroid hormone homeostasis (Veldhoen et al., 2006). Moreover, triclosan can accumulate in various aquatic organisms, and has been found highly toxic to certain types of algae and fish (Orvos et al., 2002). Triclosan may induce development of bacterial resistance to drugs (McMurry et al., 1998). Of particular concern is the sewage sludge, where an abundance of pathogens and multiple antibiotics often coexist (Heidler and Halden, 2007). The continued use and accumulation of triclosan in the environment have led to regulatory actions by the U.S. FDA (2013).

Various oxidation processes have been investigated to degrade triclosan in drinking water and wastewater plants, including chlorine oxidation, ozonation, and sunlight or UV photodegradation (Inaba et al., 2006; Latch et al., 2005; Rule et al., 2005). However, in addition to the limited effectiveness, these technologies often produce toxic byproducts or intermediates

(e.g., 2,4-dichlorophenol, 2,8-dichlorodibenzo-p-dioxin). Consequently, more cost-effective techniques are needed to mitigate the toxic effects of triclosan.

Catalytic hydrodechlorination is a common reductive degradation process where chlorinated organic compounds are reduced by hydrogen gas with inorganic chloride ions released. To speed up the reaction rate and minimize production of toxic byproducts, various catalysts are often employed. Palladium (Pd) has been one of the most frequently used catalysts in catalytic hydrodechlorination for its high catalytic efficiency under ambient pressure and temperature. It is well known that Pd can facilitate formation of highly reactive atomic hydrogen and the C−Cl bond cleavage (Chen et al., 2002; Lowry and Reinhard, 2001).

To enhance the catalyst activity and facilitate water treatment uses of the catalyst, elemental Pd particles are often loaded on macro-scale supporting materials. For instances, activated carbon (AC) and alumina (Al_2O_3) have been most commonly employed as the supports (Chaplin et al., 2012; Diaz et al., 2011; Zhang et al., 2013).

Conventionally, Pd particles are prepared by reducing ionic Pd species in solution, and then loaded on a support via the incipient wetness impregnation method (Bacik et al., 2012). However, the particles in aqueous solution tend to aggregate, and the aggregates can hardly be uniformly loaded on porous supports. Moreover, due to lack of specific interactions between Pd and the supports, the loaded Pd particles are prone to leaching. For instance, Yuan and Keane (2004) tested AC and alumina supported Pd, and observed that 34% of Pd leached out from AC-Pd and 10% from alumina-Pd. To enhance Pd activity and minimize Pd leaching, high temperature calcination is often practiced. However, calcination not only costs a large amount of energy, but also is less applicable to AC and polymeric materials.

Compared to AC and alumina, functional polymeric resins may offer some unique advantages when used for preparing supported catalysts. First, functional polymers carry uniformly distributed functional groups that can strongly adsorb the precursor ionic Pd species, which is an essential step for subsequent uniform loading of Pd nanoparticles. Second, the adsorbed Pd species can be easily reduced to elemental Pd, which allows the nanoparticles to be generated evenly and in situ. Third, the polymeric template may serve as a solid stabilizer preventing the nanoparticles from aggregation and maximizing the catalytic activity. Fourth, the polymer matrix and functional groups can interact strongly with Pd, resulting in firm immobilization of the nanoparticles and minimal Pd leaching. This also eliminates the need for high temperature calcination. Fifth, the Pd loading can be easily manipulated by controlling the ion-exchange uptake of the precursor Pd species. Last, there have been diverse types of ion exchange resins available on the market with a wide range of physical-chemical characteristics (functionality, porosity, matrix hydrophobicity, and surface area), allowing for selecting the optimal resins for the target contaminants. Gasparovicova et al. (2006) prepared a Pd−Cu bimetallic catalyst supported on strong acid cation resins to reduce nitrates, and observed improved selectivity toward N_2 production and undetectable Pd leaching.

In this study, a new class of resin-supported Pd catalysts were prepared using two widely used strong base anion (SBA) exchange resins, Amberlite IRA-900 and Amberlite IRA-958, through a two-step process (i.e., ion-exchange uptake and subsequent reduction), and the catalysts were then characterized and tested for catalytic hydrodechlorination of triclosan. The specific objectives were to: 1) Prepare and characterize the resin-supported Pd catalysts; 2) Determine the effects of Pd loading and type of resin matrices on the effectiveness of catalytic hydrodechlorination; 3) Test the life-time and reusability of the catalysts, and resistibility to

chloride poisoning, organic fouling and pH fluctuation; and 4) Identify the reaction pathway of catalytic hydrodechlorination of triclosan. To the best of our knowledge, there has been very limited information reported on reductive degradation of triclosan.

2. Materials and methods

2.1 Materials

Section S1 in Supporting Information (SI) gives information on chemicals used in this study. Two widely used macroporous SBA resins, Amberlite IRA-900 and IRA-958 (both in Cl^- form) (Dow Chemical Company, Philadelphia, PA, USA) were purchased from Sigma-Aldrich. Both resins contain quaternary amine functional groups and nearly the same ion exchange capacity, but differ in the polymer matrices (polystyrene for IRA-900 and polyacrylic for IRA-958). **Table 1** lists the salient properties of the two resins. Before use, the resins were conditioned following the procedure of cyclic exhaustion with 1 M sodium hydroxide, 1 M hydrochloric acid, 1 M NaCl, and DI water rinsing successively, and then air-dried (Xiong et al., 2007).

2.2 Preparation of resin-supported catalysts

The resin-supported Pd catalysts were prepared by a two-step process. First, an anionic form of Pd precursor ($PdCl_4^{2-}$) was absorbed on the resins through the following ion-exchange reactions:

$$R\text{-}(N^+Cl^-)_2 + PdCl_4^{2-} \leftrightarrow R\text{-}N_2\text{-}PdCl_4^{2-} + 2Cl^- \quad (1)$$

where R- represents the polymer matrix. Typically, to achieve 2.0 wt.% Pd loading, a 100 mL solution containing 21.5 mg/L of $PdCl_4^{2-}$-Pd and 1 g/L NaCl was mixed with a resin at a solution-to-resin ratio of 1 (L):1 (g) and equilibrated on a shaker (150 rpm) for 72 h (to reach equilibrium). Then the supernatant was decanted, and 5 mL of a borohydride solution (0.86 g/L)

was added to the Pd-laden resins dropwise. Pd(II) was reduced to Pd(0) through the following reaction under shaking (150 rpm) for 20 min:

$$PdCl_4^{2-} + 2BH_4^- + 6H_2O \rightarrow Pd^0 + 2B(OH)_3 + 4Cl^- + 7H_2\,(g) \quad (2)$$

The resulting resin-supported Pd catalysts contained 2.0 wt.% Pd, and are designated as Pd(2.0)@IRA-900 or Pd(2.0)@IRA-958, respectively. The catalysts were rinsed with DI water and then air-dried before use. For comparison, the catalysts were also prepared with Pd loadings ranging from 0.2 to 11.2 wt.% following the same procedure and according to the $[PdCl_4]^{2-}$ adsorption (ion-exchange) isotherms (**Figure S1** in SI).

2.3 Catalysts characterization

The topography and morphology of the resin-supported Pd catalysts were investigated by scanning electron microscopy (SEM, JSM-7000F, JEOL, USA), coupled with energy-dispersive X-ray spectroscopy (EDS, INCA X-Sight, Oxford Instruments) for elemental composition analysis. To determine the distribution of Pd loaded inside a resin bead and the internal morphology, selected resin beads were first bisected, and then the cross-sections subjected to the SEM and EDS analyses. Transmission electron microscopy (TEM) (Tecnai30 FEG microscopy, FEI, USA) analysis was performed to determine the morphology and approximate particle size of the supported Pd particles following the methods in (Bacik et al., 2012). Powder X-ray diffraction (XRD) patterns of the catalysts were obtained with a Bruker D2 PHASER powder diffractometer (Bruker AXS, Germany) using Cu *Kα* radiation (λ = 1.5418 Å) at a scan rate (2θ) of 4°/min.

2.4 Catalytic hydrodechlorination of triclosan

Batch kinetic experiments were conducted in duplicate to test the effectiveness of the supported Pd catalysts for hydrodechlorination of triclosan in aqueous solution. First, 0.1 g of a

resin-supported Pd catalyst was mixed with 100 mL of DI water in a 127 mL amber serum bottle. Then the mixture was purged with hydrogen gas for 25 min to obtain a H_2-saturated solution (H_2 solubility ≈1.6 mg/L at 20°C) with the headspace (~27 mL) filled with H_2. Upon saturation, the bottle was quickly capped with an open-top screw cap with PTFE-lined septa. Hydrodechlorination of triclosan was then initiated by injecting 100 µL of the triclosan stock solution into the bottle using a gas-tight glass syringe to yield an initial triclosan concentration of 10 µM (2.9 mg/L). The reactor was then flat-mounted on a shaker and kept mixing at 150 rpm at room temperature (20±1 °C). At selected times, 1 mL of the solution was sampled and filtered through a 0.22 µm Teflon syringe filter. The filtrates were then analyzed for triclosan remaining. Two types of control tests were conducted to quantify the mass loss of triclosan, one was with the solution only, and the other was with hydrogen gas added but without the catalysts. To test pH effects, the kinetic tests were conducted at pH 3.0-8.8, which was pre-adjusted using dilute HCl or NaOH. The variation of solution pH was <0.3 during the experiments in all cases.

Because of the hydrophobic nature of the resin matrices, triclosan in the aqueous phase can be removed due to both adsorption and chemical transformation. To gauge triclosan adsorption on the resins, the catalytic hydrodechlorination was terminated at various times. Upon withdrawal of the solution (~99 mL), the resins were extracted using 30 mL of methanol to extract adsorbed triclosan in the resin phase. The extraction was performed under shaking (250 rpm) for 24 h at room temperature (20±1˚C). Control tests indicated that the extraction method can recover 96±2 % and 97±2 % triclosan from IRA-900 and IRA-958, respectively.

Experimental methods on testing and analyzing the humic acid (HA) effect, hydrodechlorination byproducts, chloride production and chlorine balance, and catalysts reuse and lifetime are provided in Sections S2-S5 in SI.

2.5 Chemical analysis

Triclosan was analyzed with an HP Agilent 1260 Infinity High Performance Liquid Chromatography (HPLC) system following the method by Zhang and Huang (2003). Section S6 in SI presents details of the method and methods for analyzing total dissolved Pd, the hydrodechlorination byproducts and chloride.

3. Results and discussion

3.1 Crystallography, morphology, and chemical compositions of catalysts

Figure 1 shows the XRD patterns of Pd(2.0)@IRA-900 and Pd(2.0)@IRA-958 before and after eight reaction cycles of hydrodechlorination. No peaks were detected in the diffractograms for both resins, which is consistent with the amorphous nature of the polymeric matrices. In contrast, three peaks ($2\theta \approx 39.4°$, 46.1°, and 67.7°) were observed upon Pd loading. These peaks are assigned to the 111, 200 and 220 crystal planes of the face centered cubic (fcc) crystallographic structure of Pd, respectively (JCPDS No. 05-0681), confirming Pd nanoparticles were successfully loaded onto resins. Comparing the freshly prepared Pd catalysts with those after eight consecutive hydrodechlorination cycles, there is no significant change of the Pd peaks, indicating good stability of the catalysts after repeated uses.

Figure 2 shows the SEM images of the cross-section of Pd loaded resins at 100x and 30,000x magnifications. The high magnification SEM images show a macroreticular internal structure of the resins, and the macropores (i.e., those larger than 50 nm) result from “glueing” of polymer nodules (D’Archivio et al., 2000). It is evident that IRA-900 contains much more macropores between the nodules than IRA-958. Consistent with the SEM images, IRA-900 was reported to have an average pore diameter of 37.2 nm, which is ~6 times larger than that for IRA-958 (6.46 nm) (Kołodyńska, 2010; Schouten et al., 2007). Moreover, the BET surface area

of IRA-900 (22 m^2/g) is ten times higher than IRA-958 (2.03 m^2/g) (Delgado et al., 2007; Kołodyńska, 2010). Compared with other inorganic supports, the BET surface area of the resins is relative low. For instance, the BET surface area for alumina (Al_2O_3) supported Pd was 92 m^2/g (Zhang et al., 2013), and that for AC supported Pd may reach 1011 m^2/g (Diaz et al., 2011).

Radial distribution of Pd nanoparticles at the surface and cross-section of the resins was analyzed by EDS scanning of 11 points, which were distributed along the radius in the upper and right direction (**Figures 2a-2b**). **Figure 3** shows the EDS results, where the Pd distribution was plotted as Pd percentage relative to Cl (note: Cl^- was considered evenly adsorbed on the resins). The results indicate that Pd distribution was radially symmetrical, and Pd was quite uniformly distributed inside the resins with an average Pd/Cl = 8.0% and 9.2% for IRA-900 and IRA-958, respectively. However, at the peripheral surface of resins, higher Pd loadings were observed, with an average Pd/Cl = 13.6 and 19.6 % for IRA-900 and IRA-958, respectively.

Gross et al. (2010) prepared palladium catalysts supported on weak anion exchange resins using hydrazine as the reducing agent, and they found that the Pd particles were concentrated in the 10% outer shell. Corain and Kralik (2000) claimed that well swelling media (e.g., ethanol) and high concentrations of reducing agents tend to distribute the particles more evenly. In our case, the macroreticular structure and the evenly distributed functional groups of the resins resulted in an initial uniform loading of Pd precursor ions. The use of the strong reducing agent ($NaBH_4$) resulted in nearly mono-dispersed nanoparticles that are evenly immobilized on the pore walls of the resins. The higher Pd loading on the peripheral surface is attributed to the higher precursor concentration at the outer sphere of the resin beads as well as the residual Pd precursor anions in the outer-sphere liquid film.

Based on the Cl^- concentration (**Table 1**) and the average Pd/Cl percentages (8.0% and 9.2%), the Pd loadings are estimated to be 26 and 22 mg/g-resin for IRA-900 and IRA-958, respectively. These values are reasonable compared with the targeted 2.0 wt.% Pd loading.

Figure 4 shows TEM images of the Pd particles and their distribution on the resins. Individual nanospheres or irregular clusters were observed for both cases, and the mean diameter of the primary nanoparticles were 3.7±1.2 nm (mean±standard deviation) and 4.6±1.8 nm for Pd(2.0)@IRA-900 and Pd(2.0)@IRA-958, respectively. **Figure S2a** in SI shows the particle size distribution. Based on t-test, the Pd particle sizes for the two resins were significantly different (p = 0.0005). However, some larger aggregates (20-40 nm diameter) were observed on IRA-958 (Figures 4c-4d). The crystal lattice distance was measured to be 0.22 nm, which is consistent with the crystalline of Pd(111) (Mazumder and Sun, 2009). EDS analyses confirmed the dark dots in the TEM images were Pd nanoparticles (**Figure S2b** in SI).

3.2 Effect of Pd loading on hydrodechlorination of triclosan

Batch kinetic tests of hydrodechlorination of triclosan were carried out under different Pd loadings. The control tests indicated that H_2 gas alone removed only 7% of triclosan in 120 min. The heterogeneous catalytic reaction is interpreted by Langmuir-Hinshelwood (L-H) model (Rizzo et al., 2009) :

$$r = -\frac{dC}{dt} = k_{rxn}\left(\frac{K_{ads}C}{1+K_{ads}C}\right) \quad (3)$$

where r is the reaction rate (mg/L/min), k_{rxn} is the rate constant (mg/L/min), and K_{ads} (L/mg) is the equilibrium constant of adsorption, C (mg/L) is the aqueous phase concentration of triclosan. For dilute aqueous solutions, $K_{ads}C$ <<1, Eqn (3) is simplified to the pseudo first-order rate law:

$$-\frac{dC}{dt} = k_{rxn}K_{ads}C = k_{\mathrm{a}}C \quad \text{or} \quad ln\frac{C}{C_0} = -k_{\mathrm{a}}t \quad (4)$$

$$k_{\mathrm{a}} = k_{\mathrm{obs}}C_{\mathrm{Pd}} \quad (5)$$

where C_0 (mg/L) is the initial concentration of triclosan, k_a (min^{-1}) is the apparent rate constant, k_{obs} (L/g/min) is the observed rate constant, which is obtained by normalizing the k_a to the dosage of Pd (C_{Pd} in g/L). **Figure 5** plots the kinetic data according to the linearized pseudo first-order equation. **Table 2** lists the best-fitted rate constants at various Pd loadings.

It is evident from **Figure 5** that without Pd loading, IRA-900 offers much greater adsorption rate and capacity for triclosan than IRA-958, and the k_a value (0.021 min^{-1}) for IRA-900 is 10 times greater than that (0.002 min^{-1}) for IRA-958. This is consistent with the matrix hydrophobicity of the resins. Given the rather hydrophobic nature of triclosan ($\log K_{OC}$ = 3.8−4.0) (Lindström et al., 2002), the more hydrophobic polystyrene matrix of IRA-900 adsorbs triclosan more favorably than the polyacrylic matrix of IRA-958. The loading of 0.2 wt.% of the Pd nanoparticles increased the rate constant by 24% (to 0.026 min^{-1}) for Pd@IRA-900 and 11 times (to 0.024 min^{-1}) for Pd@IRA-958. This observation suggests that while Pd@IRA-900 may remove triclosan through both adsorption and catalytic hydrodechlorination, Pd@IRA-958 works almost completely by catalytic hydrodechlorination. More details on the effect of the supporting resins are discussed in Section 3.3.

For Pd@IRA-900, increasing the Pd loading from 0.1 to 10.8 wt.% had statistically insignificant (p = 0.11) effect on the apparent rate constant, which remained at approximate 0.025±0.003 min^{-1} (**Table 2**). In contrast, for IRA-958, increasing the Pd loading from 0.1 to 7.8 wt.% kept increasing the rate constant from 0.012 to 0.037 min^{-1} (~3 times). This observation indicates that the strong adsorption by IRA-900 is limiting the intraparticle mass transfer rate of triclosan, i.e., the surface diffusion is likely limiting the hydrodechlorination process for Pd@IRA-900, while the Pd-facilitated reaction plays an important role for Pd@IRA-958 in the tested Pd-loading range. Further increasing Pd from 7.8 to 11.2 wt.% on IRA-958 showed no

more effect on the reaction rate, indicating the rate limiting step is shifted to other mechanisms (e.g., diffusion). Nutt et al. (2005) studied effect of Pd loading on trichloroethylene (TCE) hydrodechlorination using a Pd-on-Au bimetallic catalyst, and found that multiple layers of Pd particles were formed at the support surface at elevated Pd loadings. Our SEM images (**Figure S3**) appear to support the assertion that layered Pd patches may form on the supports at high Pd loadings (~11 wt.%). The Pd accumulation may block the accessibility of the interior Pd sites of the porous support, resulting in a decrease in the specific surface area and the overall catalytic efficiency.

On the other hand, when the Pd-normalized rate constants (k_{obs}) are compared, the lower Pd loading (0.1 wt.% and 0.2 wt.%) gives the higher k_{obs} value (**Table 2**) for both types of resins.

3.3 Effect of supports on hydrodechlorination of triclosan

As stated earlier, the resin matrices can adsorb triclosan. In particular, adsorption by the polystyrene matrix of IRA-900 may affect the hydrodechlorination rate. To acquire further insight into the role of adsorption, triclosan removal due to adsorption and reaction was quantified by measuring triclosan in the solid phase and in the aqueous phase. **Figure 6** shows concentration histories of triclosan in the resin and the aqueous phases during the 120 min hydrodechlorination. It is evident from **Figure 6a** that at the 0.2 wt.% Pd loading, up to 20% of initial triclosan was detected in the Pd(0.2)@IRA-900 phase, which was then rapidly and nearly completely degraded. In contrast, for Pd(0.2)@IRA-958, no adsorbed triclosan was detected at 0.2 wt.% Pd loading, indicating triclosan removal was solely due to reaction. When the Pd loading was increased to 2.0 wt.%, no solid-phase triclosan was detected for both resins (**Figure 6c**).

For adsorption of contaminants onto polymeric resins, intraparticle diffusion is often the rate limiting step (Zhao and Pignatello, 2004). For both Pd@IRA-900 and Pd@IRA-958, intraparticle diffusion can include both pore diffusion and surface diffusion. As most of the adsorption sites are not covered by the Pd nanoparticles, a good fraction of triclosan molecules will be first adsorbed on the resins' surface and then be degraded by the reactive atomic hydrogen produced by the Pd nanoparticles (He and Zhao, 2008). As the pore size of IRA-900 is 4.8 times larger than that of IRA-958 (**Table 1**), the pore diffusion rate for the former is faster than for the latter. On the other hand, as the polystyrene matrix adsorbs triclosan much more favorably than the polyacrylic matrix, triclosan molecules are more strongly adsorbed on the IRA-900 before they are hydrodechlorinated, and the adsorption retards the surface diffusion to a greater extent than for IRA-958. Consequently, surface diffusion is likely the rate-limiting step for Pd@IRA-900. In contrast, for Pd@IRA-958, adsorption is much weaker, and thus plays much less a role, i.e., the production of atomic hydrogens and degradation reaction control the removal rate. At elevated Pd loadings (e.g., 2.0 wt.%), the surface diffusion limitation is relaxed as more Pd nanoparticles become available and more atomic hydrogen is produced. Consequently, no triclosan residual was detected in the resin phase (**Figure 6c**). However, detailed mechanisms on the mass transfer and production of atomic hydrogen are yet to be investigated in the future.

Figure 6d shows that despite the different adsorption and mass transfer mechanisms, the overall removal rates of triclosan for both Pd(0.2)@IRA-900 and Pd(0.2)@IRA-958 were quite comparable, though Pd@IRA-958 outperformed Pd@IRA-900 at elevated Pd loadings (**Table 2**). It is noteworthy that the specific surface area for IRA-958 (2.03 m^2/g) is 10 times smaller than

319 that of IRA-900 (22 m^2/g) (**Table 1**). As a result, when loaded with the same mass of Pd, the
320 surface density of the Pd nanoparticles is higher on IRA-958, which is in favor of the reaction.

321 **3.4 Effects of pH and chloride**

322 To study the pH effect, the hydrodechlorination experiments were conducted at pH 3.0-8.8.
323 **Figure S4** shows that the fastest reaction was observed at pH 5.0. Increasing pH from 5.0 to 8.8
324 lowered the k_{obs} value from 1.25±0.06 to 0.88±0.03 L/g/min for Pd(2.0)@IRA-900, and from
325 1.6±0.1 to 0.93±0.02 L/g/min for Pd(2.0)@IRA-958. Conversely, lowering solution pH from 5.0
326 to 4.0 only slightly reduced the reaction rate. However, further decreasing pH from 4.0 to 3.0
327 diminished the k_{obs} from 1.11±0.05 to 0.85±0.05 L/g/min for Pd(2.0)@IRA-900 and 1.39±0.02
328 to 0.82±0.01 L/g/min for Pd(2.0)@IRA-958. The higher reactivity of Pd catalysts at mildly
329 acidic pH is attributed to the increased formation of atomic H due to elevated H^+ concentration at
330 lower pH (Liu and Wang, 2014; Zhao et al., 2014). In addition, solution pH also influence
331 catalyst surface properties and speciation of triclosan. The point zero charge of the
332 Pd(2.0)@IRA-900 and Pd(2.0)@IRA-958 was determined to be 4.5 and 5.4 following the
333 titration method, respectively (**Figure S5**). The pK_a value of triclosan was reported to be 7.9
334 (Latch et al., 2005). As such, the surface of catalysts becomes increasingly negatively charged at
335 pH above 5, and the adsorption of triclosan becomes less favorable at rising pH due to the charge
336 exclusion effect. At pH >8, the phenolic groups of triclosan become largely deprotonated,
337 invoking a stronger electrostatic repulsion with the negatively charged catalysts. At the
338 extremely acidic pH 3.0, ~0.5 wt.% of Pd loaded was dissolved, resulting in some reactivity loss.
339 Earlier, Liu and Wang (2014) studied hydrodechlorination of 4-chlorophenol using a PdCoB
340 catalyst and observed similar deactivation phenomenon at pH 2.5. Extremely high concentrations

of H^+ may also affect the reaction through product-inhibition since hydrogen ions are also hydrodechlorination products (Section 3.6).

Researchers have reported poisoning effects of halide ions (e.g., Cl^- and Br^-) on Pd catalysts (Ordóñez et al., 2010; Urbano and Marinas, 2001). To gauge the Cl^- effect, 10 mM NaCl was added in eight consecutive batch kinetic tests. **Figure S6** shows that in the presence of the high salt concentration, k_{obs} was decreased from 1.25 to 0.94 L/g/min for Pd(2.0)@IRA-900, and from 1.6 to 1.28 L/g/min for Pd(2.0)@IRA-900 in the first run, respectively, and to 0.86 L/g/min and 1.24 L/g/min after 8 consecutive runs. High concentrations of halide ions are able to form stable complexes with Pd^{2+}, which will promote oxidation of Pd^0 to Pd^{2+} and diminish its catalytic activity (Ordóñez et al., 2010; Urbano and Marinas, 2001). This phenomenon gives rise to an undesired self-inhibition mechanism when chloride ions are present as a reduction byproduct.

Nonetheless, both Pd(2.0)@IRA-900 and Pd(2.0)@IRA-958 were able to perform well in the presence of high concentrations of NaCl, with k_{obs} being decreased by only 31% and 23%, respectively, after 8 consecutive runs (most drop occurred in the first run). Between the two catalysts, Pd(2.0)@IRA-958 appeared more resistant to Cl^-, which can be attributed to its relatively larger Pd particle size. Larger particles are less reactive, but less vulnerable the chloride effect. Aramendia et al. (1999) claimed the ability of Pd to adsorb hydrogen and to form a β-hydride phase may have an important role in the activity/selectivity of alumina-supported Pd. They also reported that larger palladium particles show a better resistance to passivation, and they claimed that the byproduct halide ions can diffuse into the micropores of larger Pd aggregates, thereby vacating the outer surface for further reaction. Gigola et al. (1986) reported that larger Pd particles are more likely to form the β-hydride species, which is often associated

with a larger H_2 uptake at room temperature. Likewise, Estellé et al. (1996) hypothesized that small metal particles cause hydrogen to dissociate less effectively than large particles.

3.5 Effect of humic acid

Dissolved organic matter (DOM) inhibition has been reported to be a major issue for organics degradation by Pd-based catalysts (Chaplin et al., 2006; Zhang et al., 2013). **Figures 7a-7b** show linearized hydrodechlorination kinetics of triclosan by Pd(2.0)@IRA-900 and Pd(2.0)@IRA-958 in the presence of various concentrations of Fluka HA measured as total organic carbon (TOC). Evidently, the presence of HA at 10 mg/L as TOC only slightly reduced the k_{obs} value from 1.25±0.06 to 1.18±0.04 L/g/min for Pd(2.0)@IRA-900, and from 1.6±0.1 to 1.5±0.2 L/g/min for Pd(2.0)@IRA-958, which is statistically insignificant for Pd(2.0)@IRA-958 (p value = 0.09). When the HA concentration was doubled to 20 mg/L as TOC, the k_{obs} value was decreased to 0.95±0.04 and 1.24±0.01 L/g/min for Pd(2.0)@IRA-900 and Pd(2.0)@IRA-958, respectively; and when HA was tripled to 30 mg/L as TOC, the k_{obs} value was further decreased to 0.9±0.2 and 1.17±0.06 L/g/min, i.e., a drop of 28% for Pd(2.0)@IRA-900 and 27% for Pd(2.0)@IRA-958 compared to those without HA. Namely, both IRA-900 and IRA-958 supported Pd catalysts showed excellent resistance to organic fouling/poisoning at TOC<10 mg/L, and both catalysts showed similarly good resistance at extremely high TOC concentrations.

Figure S7 compares the effects of Fluka HA (FHA) and Leonardite HA (LHA) at 30 mg/L as TOC on the triclosan removal rates. For both Pd(2.0)@IRA-900 and Pd(2.0)@IRA-958, the two HAs showed nearly identical effects on the removal kinetics (p > 0.2). **Figure S8** shows the effects of FHA at 30 mg/L as TOC on the removal rate of triclosan at a 10 times lower concentration (0.29 mg/L). The presence of 30 mg/L FHA lowered the k_{obs} value from 1.32±0.02 to 0.96±0.04 L/g/min (by 27%) for Pd(2.0)@IRA-900 and from 1.47±0.02 to

1.18±0.01 L/g/min (by 20%) for Pd(2.0)@IRA-958. The rate drop values are either comparable (for Pd(2.0)@IRA-900) or much lower (for Pd(2.0)@IRA-958). The results indicate that the supported catalysts can perform well at trace levels of triclosan and in the presence of unusually high concentrations of DOM. In fact, as the concentration of triclosan is lowered, the Pd-to-triclosan ratio is increased, resulting in less inhibitive effect of DOM.

HA can compete with triclosan for atomic hydrogen ($H^{\bullet}$), thus inhibiting the hydrodechlorination rate (Zhu et al., 2008). In addition, HA may adsorb onto the active Pd surface sites, causing catalyst fouling (Chaplin et al., 2006). Zhang et al. (2013) investigated hydrodechlorination of trichloroethylene with alumina-supported Pd catalysts, and reported a ~88% loss of reaction rate in the presence of 30 mg/L of HA. Likewise, Chaplin et al. (2006) reported the reduction rate of NO_3^- decreased by 84% in the presence of 3.3 mg/L of HA using a Pd-Cu/Al_2O_3 catalyst. Evidently, the resin supports in this work render much greater tolerance to HA fouling, which can be attributed to: 1) much lower HA uptake by the resins then other supports such as AC and activated alumina, and 2) the pore size exclusion effect, i.e., the macroreticular pore structure for both IRA-900 and IRA-958 prevents HA macromolecules from reaching the Pd nanoparticles inside the resin beads. In the presence of 30 mg/L of HA, Pd(2.0)@IRA-900 and Pd(2.0)@IRA-958 removed 37% and 24% of HA, respectively, after 2 h.

To further investigate the DOM effect, consecutive exhausting runs of catalytic hydrodechlorination were conducted in the presence of 30 mg/L TOC. **Figures 7c-7d** show the linearized kinetic profiles in Runs 2, 4 and 6. The k_{obs} values for Runs 2, 4, 6 were 0.70±0.2, 0.60±0.1, and 0.57±0.07 L/g/min for Pd(2.0)@IRA-900, and 0.98±0.07, 0.93±0.01, 0.90±0.03 L/g/min for Pd(2.0)@IRA-958. After 6 runs, the k_{obs} values decreased by 39% and 27% compared with the first runs for Pd(2.0)@IRA-900 and Pd(2.0)@IRA-958. In fact, IRA-958 was

manufactured to resist organic fouling for its hydrophilic and macroporous/macroreticular matrix. In addition, the smaller pore size of IRA-958 will exclude more HA molecules and result in less fouling. The results indicate that over prolonged exposure to very high concentrations (e.g., 30 mg/L) of DOM, the catalytic activity may gradually lessen due to slow diffusion and adsorption of DOM molecules.

3.6 Triclosan hydrodechlorination pathway

Unlike conventional oxidative degradation of triclosan, which often produces highly toxic byproducts, such as chlorodioxins and chlorophenol (Latch et al., 2005; Rule et al., 2005), the catalytic hydrodechlorination was expected to give innocuous reaction products. **Figure S9** shows the GC/MS chromatograms obtained during the catalytic hydrodechlorination of triclosan at various reaction times (10 min to 24 h). **Figure S10a** shows the relative GC/MS peak area throughout the reaction time, and **Figure S10b** gives the MS spectra with the m/z values. The differences between the measured and theoretical masses were <0.5%. It is evident that triclosan was rapidly dechlorinated. At 10 min, ~30% of initial triclosan was degraded. The major intermediate product (P1 in **Figure S9** in SI) was identified as 2-phenoxyphenol with a m/z value of 186.00, which was also reported by others (Bokare et al., 2010; Nakayama et al., 2008). In addition, three other byproducts were detected, including two of the 2-chlorinated isomers ($C_{12}H_8Cl_2O_2$), and one 1-chlorinated compound ($C_{12}H_9ClO_2$) (Figures S9 and S10 in SI). At 30 min, the chlorinated byproducts were further dechlorinated, and complete dechlorination of triclosan was achieved within 2 h, where P1 was the major product with a small amount of P2. At 4 hour, P1 was further converted to P2, and two new peaks P3 and P4 appeared. P2 has an m/z value of 190.00, but its molecular has not been reported. Based on the mass spectrum analysis (**Figure S10b**) and the peak area trend (**Figure S10a**), P2 is suggested as a

hydrogenation product of P1. To confirm the most possible structure of P2, the condensed Fukui function (CFF) was employed to study the regioselectivity of the H radical addition to P1 (Section S7 of SI). The results indicate that the Carbons-1, 2, 5, and 6 were the most reactive sites for further H radical additions (Figure S11), i.e., P2 is most likely 6-phenoxycyclohex-3-enol (M.W.= 190.2). The structures for P3 and P4 were not identified in this work. Further conversions of P1 and P2 to P3 and P4 were observed at 9 h. Sun et al. (2007) observed catechol and resorcinol decomposed ring-opened products in hydrodechlorination of *o*-chlorophenol.

Based on the intermediation products analysis, the catalytic hydrodechlorination pathway of triclosan by resin-supported Pd catalysts is schemed in **Figure 8**, and the triclosan hydrodechlorination can be described by the following reactions:

$$C_{12}H_7Cl_3O_2+H_2 \xrightarrow{Pd} C_{12}H_8Cl_2O_2+Cl^-+H^+ \quad (6)$$

$$C_{12}H_8Cl_2O_2+H_2 \xrightarrow{Pd} C_{12}H_9ClO_2+Cl^-+H^+ \quad (7)$$

$$C_{12}H_9ClO_2+H_2 \xrightarrow{Pd} C_{12}H_{10}O_2+Cl^-+H^+ \quad (8)$$

$$C_{12}H_{10}O_2+2H_2 \xrightarrow{Pd} C_{12}H_{14}O_2 \quad (9)$$

It is noteworthy that the hydrogen supply in the system (H_2 solubility ≈1.6 mg/L at 20°C) was more than 10 times the stoichiometric demand, which assures abundant hydrogen supply for the catalytic hydrodechlorination.

To confirm the dechlorination completeness, chlorine mass balance was vetted in the system. **Figure 9** shows the coupled catalytic hydrodechlorination rate of triclosan and the production rate of Cl^- by Pd(2.0)@IRA-958. Evidently, the dechlorination of triclosan was nearly stoichiometrically coupled with the production of chloride. It is noted that the sum of chloride and chlorine in triclosan was slightly lower than initial total chlorine mass in the first hour or so,

455 which is attributed to the presence of minor chlorinated byproducts during initial reaction stage
456 (**Figure S9**). After 1 h, ~100% chlorine mass balance was observed, thus confirming complete
457 dechlorination of chlorinated byproducts. Similar Cl^- production profile was observed for
458 Pd(2.0)@IRA-900 (data not shown). At equilibrium (2 h), nearly all triclosan-chlorine was
459 converted to Cl^-.

460 **3.7 Catalysts lifetime**

461 The lifetime and reusability of the resin-supported Pd catalysts were tested through eight
462 consecutive runs, where the same catalyst was repeatedly used for triclosan hydrodechlorination
463 without any treatment. **Figures 10a-10b** shows linearized hydrodechlorination kinetics of
464 triclosan in Runs 1, 4, and 8 fitted with the pseudo-first-order kinetic model. The kinetic data for
465 Runs 2, 3, 5, 6, and 7 fall between those for Runs 1 and 8 and are not shown for visual clarity.
466 After 8 repeated uses, the k_{obs} values decreased modestly from 1.25±0.06 to 1.09±0.01 L/g/min
467 for Pd(2.0)@IRA-900, and from 1.6±0.1 to 1.45±0.02 L/g/min for Pd(2.0)@IRA-958. Pd
468 leaching for both resins was undetectable (i.e., <0.03 mg/L in the aqueous phase or <0.2 wt.% of
469 Pd loaded). This observation indicates that these resins are able to facilitate firm immobilization
470 of the Pd nanoparticles. This is a major advantage over other supporting materials such as
471 activated carbon and alumina, which often require a calcination process.

472 When the two catalysts are compared, the activity drop for Pd(2.0)@IRA-900 was slightly
473 higher than that for Pd(2.0)@IRA-958(13% versus 9% based on k_{obs}). Typically, deactivation of
474 Pd catalysts is attributed to Pd leaching, Cl/S poisoning, sintering, and accumulation of reaction
475 products on the catalyst surface (Concibido et al., 2007; Janiak and Okal, 2009; Yuan and Keane,
476 2004, 2003). In our case, the effect of Pd leaching was excluded since no Pd leaching was
477 detected for both catalysts. To determine the effects of chloride and H^+, the solution pH and Cl^-

concentration in the aqueous phase were recorded during the reuse experiments **(Figures 10c-10d).** For Pd(2.0)@IRA-900, pH dropped progressively after each run cycle (from 5.1 to 3.8 after 8 cycles). However, for Pd(2.0)@IRA-958, pH remained nearly the same after 8 runs (from 5.1 to 5.2). This phenomenon can be attributed to the different matrix effects. While the hydrophobic polystyrene matrix of IRA-900 barely interacts with protons, the polyacrylic matrix in IRA-958 contains amine and carbonyl groups, both of which undergo protonation reactions at acidic pH. As a result, the IRA-958 effectively acts as a buffer holding the pH constant by taking up the H^+ produced in the hydrogenation reactions (Eqs. 5-7). The production of Cl^- for the two catalysts was comparable, as after 8 recycles the Cl^- in the aqueous phase was increased to ~12 mg/L in both cases. Another reason for the catalyst deactivation was due to hydrophobic organic products fouling (Concibido et al., 2007; Yuan and Keane, 2003). Such fouling can be more significant for hydrophobic supports. As IRA-900 more favorably adsorbs the hydrophobic reaction products than IRA-958, Pd@IRA-900 was more vulnerable to organic fouling. In terms of effects of oxidants, Pd catalysts are known to be resistant to oxidants. In fact, strong oxidants, such as $HOCl/OCl^-$, H_2O_2, and $KMnO_4$, are often employed used to regenerate sulfur-fouled Pd catalysts (Angeles-Wedler et al., 2009; Chaplin et al., 2012, 2006). However, strong oxidants should be avoided during the hydrodechlorination reaction to minimize competitive reactions. A field demonstration test by Davie et al. (2008) showed that alumina-supported Pd was able to effectively hydrodechlorinate TCE in a groundwater without removing dissolved oxygen (0.5 mg/L) and nitrate (3.2 mg/L).

4. Conclusions

For the first time, we prepared two types of supported Pd catalysts using two standard strong-base anion exchange resins (IRA-900 and IRA-958) and through an initial adsorption and

subsequent in-situ reduction of Pd. Compared to conventional supports, the resins offer some unique advantages, including: 1) controlled and uniform Pd loading/dispersion by manipulating the Pd adsorption isotherm, 2) very high catalytic activities, 3) negligible Pd bleeding, 4) high resistance to organic fouling and chloride poisoning, and 5) great reusability with low activity loss. At a Pd loading of 0.2 wt.%, both IRA-900 and IRA-958 supported Pd catalysts facilitated rapid and complete hydrodechlorination of triclosan with an observed pseudo-first-order reaction rate constant (k_{obs}) ≥12 L/g/min. With an increase in Pd loading from 0.2 to 8 wt.%, the apparent rate constant k_a was increased for IRA-958 supported catalysts while no significant change for IRA-900 supported counterparts. This observation indicates the strong adsorption is limiting the surface diffusion and thus limiting the hydrodechlorination process for Pd@IRA-900, while the Pd loading played an important role for Pd@IRA-958. Both resin-supported catalysts were highly resistant to organic fouling, with nearly no effect in the presence of 10 mg/L of HA and the k_{obs} value being decreased by only 28% and 25% at 30 mg/L HA for Pd(2.0)@IRA-900 and Pd(2.0)@IRA-958, respectively. Low concentrations of chlorinated intermediates were detected in the early stage (<1 h) of the hydrodechlorination process, which were then rapidly and completely degraded within 1 h. A non-carcinogenic and non-mutagenic antibiotic 2-phenoxyphenol and its hydrogenated products were the main byproducts from hydrodechlorination of triclosan, and most of which were further degraded in ~24 h. The resin-supported Pd catalysts displayed a long lifetime and can be reused in multiple runs without inhibitive activity loss (the k_{obs} drop in 8 consecutive runs was less than 13%). Given the diverse characteristics of ion exchange resins, the resin-supported Pd catalysts may offer some unprecedented advantages over conventional supported catalysts in environmental cleanup applications.

Acknowledgments

The research was partially funded by the USDA-AAES Hatch and Multistate program, the National Natural Science Foundation of China (41230638), and the China National Foreign Expert Agency (No. 20152029).

Appendix A. Supplementary Information

Supplementary data associated with this article are available in the online version.

References

Angeles-Wedler, D., Mackenzie, K., Kopinke, F.D., 2009. Sulphide-induced deactivation of Pd/Al_2O_3 as hydrodechlorination catalyst and its oxidative regeneration with permanganate. Appl. Catal. B Environ. 90, 613–617.

Aramendía, M.A., Boráu, V., García, I.M., Jiménez, C., Marinas, J.M., Urbano, F.J., 1999. Influence of the reaction conditions and catalytic properties on the liquid-phase hydrodebromination of bromobenzene over palladium supported catalysts: Activity and deactivation. Appl. Catal. B Environ. 20, 101–110.

Bacik, D.B., Zhang, M., Zhao, D., Roberts, C.B., Seehra, M.S., Singh, V., Shah, N., 2012. Synthesis and characterization of supported polysugar-stabilized palladium nanoparticle catalysts for enhanced hydrodechlorination of trichloroethylene. Nanotechnology 23, 294004.

Bokare, V., Murugesan, K., Kim, Y.-M., Jeon, J.-R., Kim, E.-J., Chang, Y.S., 2010. Degradation of triclosan by an integrated nano-bio redox process. Bioresour. Technol. 101, 6354–6360.

547 Chaplin, B.P., Reinhard, M., Schneider, W.F., Schüth, C., Shapley, J.R., Strathmann, T.J., Werth,
548 C.J., 2012. Critical review of Pd-based catalytic treatment of priority contaminants in water.
549 Environ. Sci. Technol. 46, 3655-3670.
550 Chaplin, B.P., Roundy, E., Guy, K.A., Shapley, J.R., Werth, C.J., 2006. Effects of natural water
551 ions and humic acid on catalytic nitrate reduction kinetics using an alumina supported
552 Pd−Cu catalyst. Environ. Sci. Technol. 40, 3075–3081.
553 Chen, N., Rioux, R.M., Ribeiro, F.H., 2002. Investigation of reaction steps for the
554 hydrodechlorination of chlorine-containing organic compounds on Pd catalysts. J. Catal.
555 211, 192–197.
556 Concibido, N.C., Okuda, T., Nishijima, W., Okada, M., 2007. Deactivation and reactivation of
557 Pd/C catalyst used in repeated batch hydrodechlorination of PCE. Appl. Catal. B Environ.
558 71, 64–69.
559 Corain, B., Kralik, M., 2000. Dispersing metal nanoclusters inside functional synthetic resins:
560 Scope and catalytic prospects. J. Mol. Catal. A Chem. 159, 153-162.
561 D'Archivio, A.A., Galantini, L., Tettamanti, E., Panatta, A., Corain, B., 2000. Metal palladium
562 dispersed inside macroporous ion-exchange resins: Rotational and translational mobility
563 inside the polymer network. J. Mol. Catal. A Chem. 157, 269–273.
564 Davie, M.G., Cheng, H., Hopkins, G.D., Lebron, C.A., Reinhard, M., 2008. Implementing
565 heterogeneous catalytic dechlorination technology for remediating TCE-contaminated
566 groundwater. Environ. Sci. Technol. 42, 8908–15.
567 Delgado, J.A., Uguina, M.A., Sotelo, J.L., Ruíz, B., Rosário, M., 2007. Separation of carbon
568 dioxide/methane mixtures by adsorption on a basic resin. Adsorption 13, 373–383.
569 Diaz, E., Mohedano, A.F., Casas, J.A., Calvo, L., Gilarranz, M.A., Rodriguez, J.J., 2011.

570 Comparison of activated carbon-supported Pd and Rh catalysts for aqueous-phase
571 hydrodechlorination. Appl. Catal. B Environ. 106, 469–475.
572 Estellé, J., Ruz, J., Cesteros, Y., Fernández, R., Salagre, P., Medina, F., Sueiras, J.-E., 1996.
573 Surface structure of bulk nickel catalysts, active in the gas-phase hydrodechlorination
574 reaction of aromatics. J. Chem. Soc., Faraday Trans. 92, 2811–2816.
575 FDA issues proposed rule to determine safety and effectiveness of antibacterial soaps, 2013.
576 URL http://www.fda.gov/NewsEvents/Newsroom/PressAnnouncements/ucm378542.htm
577 Gašparovičová, D., Králik, M., Hronec, M., Biffis, A., Zecca, M., Corain, B., 2006. Reduction of
578 nitrates dissolved in water over palladium-copper catalysts supported on a strong cationic
579 resin. J. Mol. Catal. A Chem. 244, 258–266.
580 Gigola, C.E., Aduriz, H.R., Bodnariuk, P., 1986. Particle size effect in the hydrogenation of
581 acetylene under industrial conditions. Appl. Catal. 27, 133–144.
582 Gross, M.S., Pisarello, M.L., Pierpauli, K.A., Querini, C.A., 2010. Catalytic deoxygenation of
583 water: Preparation, deactivation, and regeneration of palladium on a resin catalyst. Ind. Eng.
584 Chem. Res. 49, 81–88.
585 He, F., Zhao, D., 2008. Hydrodechlorination of trichloroethene using stabilized Fe-Pd
586 nanoparticles: Reaction mechanism and effects of stabilizers, catalysts and reaction
587 conditions. Appl. Catal. B Environ. 84, 533–540.
588 Heidler, J., Halden, R.U., 2007. Mass balance assessment of triclosan removal during
589 conventional sewage treatment. Chemosphere 66, 362–369.
590 Inaba, K., Doi, T., Isobe, N., Yamamoto, T., 2006. Formation of bromo-substituted triclosan
591 during chlorination by chlorine in the presence of trace levels of bromide. Water Res. 40,
592 2931–2937.

593 Janiak, T., Okal, J., 2009. Effectiveness and stability of commercial Pd/C catalysts in the
594 hydrodechlorination of meta-substituted chlorobenzenes. Appl. Catal. B Environ. 92, 384–
595 392.
596 Kołodyńska, D., 2010. Cu(II), Zn(II), Ni(II), and Cd(II) complexes with HEDP removal from
597 industrial effluents on different ion exchangers. Ind. Eng. Chem. Res. 49, 2388–2400.
598 Kolpin, D.W., Furlong, E.T., Meyer, M.T., Thurman, E.M., Zaugg, S.D., Barber, L.B., Buxton,
599 H.T., 2002. Pharmaceuticals, hormones, and other organic wastewater contaminants in U.S.
600 streams, 1999-2000: A national reconnaissance. Environ. Sci. Technol. 36, 1202–1211.
601 Latch, D.E., Packer, J.L., Stender, B.L., VanOverbeke, J., Arnold, W. a, McNeill, K., 2005.
602 Aqueous photochemistry of triclosan: Formation of 2,4-dichlorophenol, 2,8-
603 dichlorodibenzo-p-dioxin, and oligomerization products. Environ. Toxicol. Chem. 24, 517–
604 525.
605 Lindström, A., Buerge, I.J., Poiger, T., Bergqvist, P.A., Müller, M.D., Buser, H.R., 2002.
606 Occurrence and environmental behavior of the bactericide triclosan and its methyl
607 derivative in surface waters and in wastewater. Environ. Sci. Technol. 36, 2322–2329.
608 Liu, X., Wang, X., 2014. Highly dispersive PdCoB catalysts for dechlorination of chlorophenols.
609 J. Hazard. Mater. 274, 63–71.
610 Lowry, G. V., Reinhard, M., 2001. Pd-catalyzed TCE dechlorination in water: Effect of $[H_2](aq)$
611 and H_2-utilizing competitive solutes on the TCE dechlorination rate and product distribution.
612 Environ. Sci. Technol. 35, 696–702.
613 Mazumder, V., Sun, S., 2009. Oleylamine-mediated synthesis of Pd nanoparticles for catalytic
614 formic acid oxidation. J. Am. Chem. Soc. 131, 4588–4589.
615 McMurry, L.M., Oethinger, M., Levy, S.B., 1998. Triclosan targets lipid synthesis. Nature 394,

531–532.

Nakayama, M., Kanaya, T., Lee, J.W., Popov, B.N., 2008. Electrochemical synthesis of birnessite-type layered manganese oxides for rechargeable lithium batteries. J. Power Sources 179, 361–366.

Nutt, M.O., Hughes, J.B., Wong, M.S., 2005. Designing Pd-on-Au bimetallic nanoparticle catalysts for trichloroethene hydrodechlorination. Environ. Sci. Technol. 39, 1346–1353.

Ordóñez, S., Vivas, B.P., Díez, F. V., 2010. Minimization of the deactivation of palladium catalysts in the hydrodechlorination of trichloroethylene in wastewaters. Appl. Catal. B Environ. 95, 288–296.

Orvos, D.R., Versteeg, D.J., Inauen, J., Capdevielle, M., Rothenstein, A., Cunningham, V., 2002. Aquatic toxicity of triclosan. Environ. Toxicol. Chem. 21, 1338–1349.

Rizzo, L., Meric, S., Kassinos, D., Guida, M., Russo, F., Belgiorno, V., 2009. Degradation of diclofenac by TiO_2 photocatalysis: UV absorbance kinetics and process evaluation through a set of toxicity bioassays. Water Res. 43, 979–988.

Rule, K.L., Ebbett, V.R., Vikesland, P.J., 2005. Formation of chloroform and chlorinated organics by free-chlorine-mediated oxidation of triclosan. Environ. Sci. Technol. 39, 3176–3185.

Schouten, N., van der Ham, L.G.J., Euverink, G.J.W., de Haan, A.B., 2007. Selection and evaluation of adsorbents for the removal of anionic surfactants from laundry rinsing water. Water Res. 41, 4233–4241.

Sun, Z., Takahashi, F., Odaka, Y., Fukushi, K., Oshima, Y., Yamamoto, K., 2007. Effects of potassium alkalis and sodium alkalis on the dechlorination of o-chlorophenol in supercritical water. Chemosphere 66, 151–157.

639 Urbano, F.J., Marinas, J.M., 2001. Hydrogenolysis of organohalogen compounds over palladium
640 supported catalysts. J. Mol. Catal. A Chem. 173, 329–345.
641 Veldhoen, N., Skirrow, R.C., Osachoff, H., Wigmore, H., Clapson, D.J., Gunderson, M.P., Van
642 Aggelen, G., Helbing, C.C., 2006. The bactericidal agent triclosan modulates thyroid
643 hormone-associated gene expression and disrupts postembryonic anuran development.
644 Aquat. Toxicol. 80, 217–227.
645 Xiong, Z., Zhao, D., Harper, W.F., 2007. Sorption and desorption of perchlorate with various
646 classes of ion exchangers: A comparative study. Ind. Eng. Chem. Res. 46, 9213–9222.
647 Yuan, G., Keane, M.A., 2004. Liquid phase hydrodechlorination of chlorophenols over Pd/C and
648 Pd/Al_2O_3: A consideration of HCl/catalyst interactions and solution pH effects. Appl. Catal.
649 B Environ. 52, 301–314.
650 Yuan, G., Keane, M.A., 2003. Catalyst deactivation during the liquid phase hydrodechlorination
651 of 2,4-dichlorophenol over supported Pd: Influence of the support. Catal. Today. 88, 27–36.
652 Zhang, H., Huang, C.H., 2003. Oxidative transformation of triclosan and chlorophene by
653 manganese oxides. Environ. Sci. Technol. 37, 2421–2430.
654 Zhang, M., Bacik, D.B., Roberts, C.B., Zhao, D., 2013. Catalytic hydrodechlorination of
655 trichloroethylene in water with supported CMC-stabilized palladium nanoparticles. Water
656 Res. 47, 3706–3715.
657 Zhao, D., Pignatello, J.J., 2004. Model-aided characterization of Tenax-TA for aromatic
658 compound uptake from water. Environ. Toxicol. Chem. 23, 1592–9.
659 Zhao, W., Zhu, X., Wang, Y., Ai, Z., Zhao, D., 2014. Catalytic reduction of aqueous nitrates by
660 metal supported catalysts on Al particles. Chem. Eng. J. 254, 410–417.
661 Zhu, B.-W., Lim, T.-T., Feng, J., 2008. Influences of amphiphiles on dechlorination of a

662 trichlorobenzene by nanoscale Pd/Fe: Adsorption, reaction kinetics, and interfacial
663 interactions. Environ. Sci. Technol. 42, 4513–4519.

Table 1. Salient properties of ion exchange resins used in this study.

Sorbent	IRA 900	IRA 958
Description	SBA resin	SBA resin
Functional Group	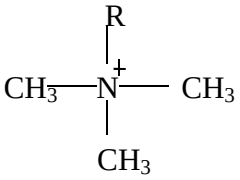	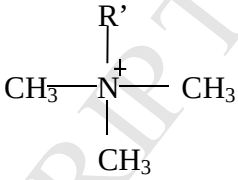
Matrix	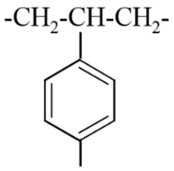 Polystyrene, macroporous	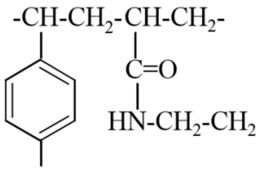 Polyacrylic, macroporous
Bead size (mm)	0.65-0.82	0.63-0.85
Cl^- Capacity (meq/g)	3.1[a]	2.2[a]
Water Content (%)	58-64	66-72
BET Surface Area (m^2/g)	22[b]	2.03[c]
Average pore diameter (nm)	37.2[d]	6.46[c]
Operating temperature (°C)	< 60	< 80

* Data obtained from Rohm and Haas Technical Bulletins unless specified otherwise; [a] From this work, determined by ion-exchange of Cl^- with SO_4^{2-}. [b] From Delgado et al. (2007). [c]From Kolodynska (2010). [d] From Schouten et al. (2007).

Table 2. Apparent and observed rate constants of triclosan removal with resin-supported Pd nanoparticles.

Resin	**Pd Loading (wt.%)**	k_a **(min^{-1})***	k_{obs} **(L/g/min)***	R^2
IRA-900	0	0.021±0.001		0.995
	0.1	0.020±0.003	20±3	0.999
	0.2	0.026±0.002	13±1	>0.999
	2.0	0.025±0.001	1.25±0.06	0.999
	4.9	0.026±0.002	0.53±0.04	0.998
	7.6	0.027±0.002	0.36±0.03	0.999
	10.8	0.028±0.002	0.26±0.02	0.999
IRA-958	0	0.002±0.000		0.702
	0.1	0.012±0.004	12±4	0.994
	0.2	0.024±0.003	12±2	0.998
	2.0	0.031±0.002	1.6±0.1	>0.999
	4.9	0.033±0.001	0.67±0.02	0.999
	7.8	0.037±0.001	0.46±0.01	>0.999
	11.2	0.037±0.004	0.31±0.03	0.999

* Errors are given as standard deviation.

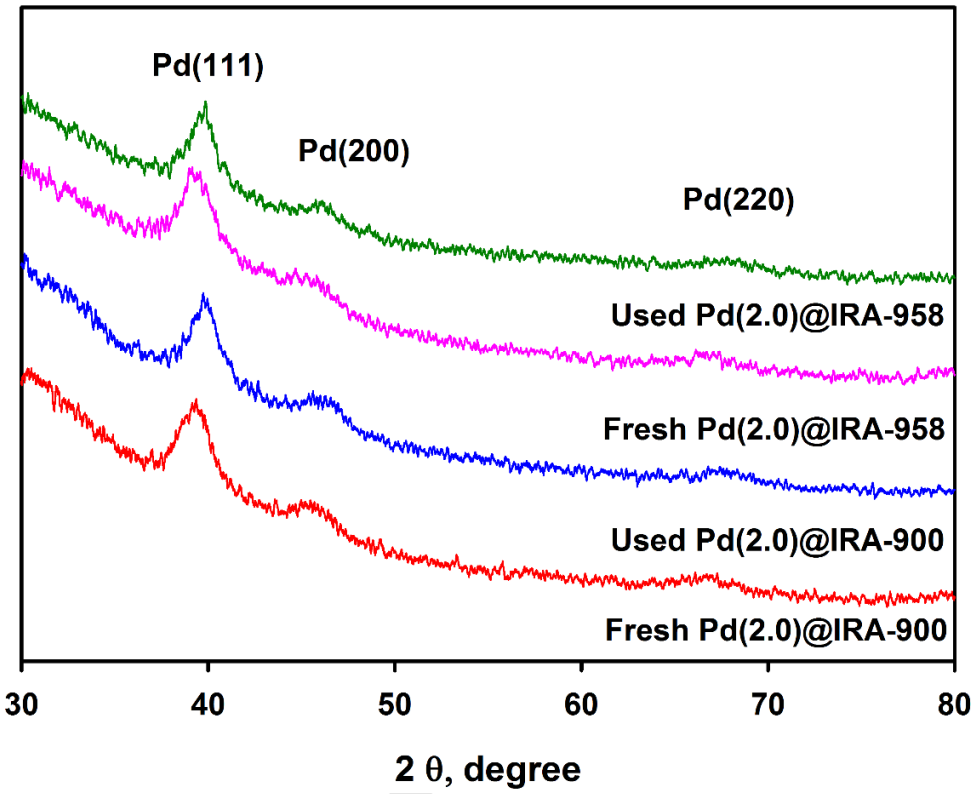

Figure 1. XRD patterns of freshly prepared resin-supported Pd catalysts and spent catalysts after 8 consecutive runs of triclosan hydrodechlorination.

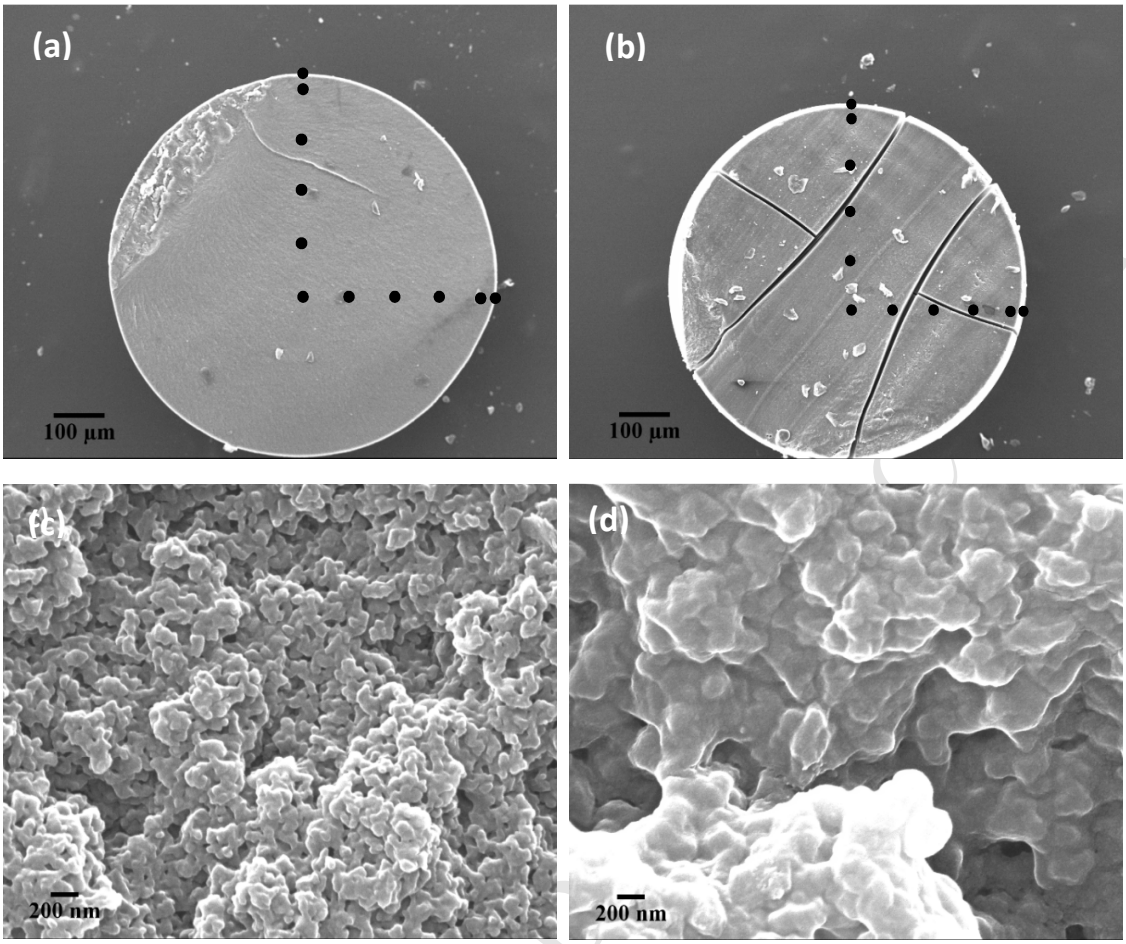

Figure 2. SEM images of cross-sections of **(a)** Pd(2.0)@IRA-900 and **(b)** Pd(2.0)@IRA-958 at low magnifications (×100), **(c)** Pd(2.0)@IRA-900 and **(d)** Pd(2.0)@IRA-958 at high magnifications (×30,000). The points in **(a)** and **(b)** indicate the EDS scanning spots.

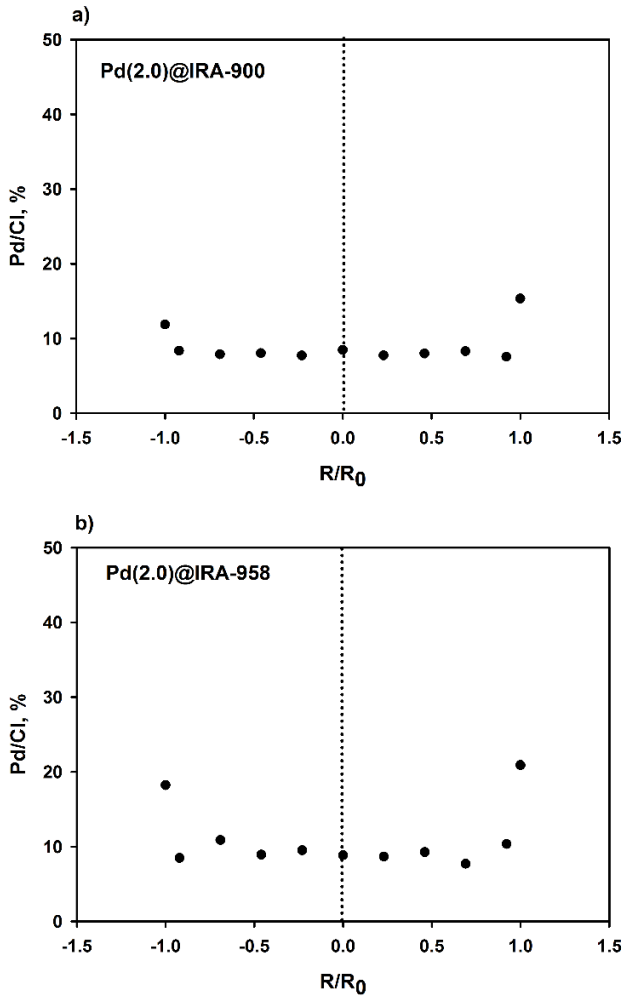

Figure 3. Radial distribution of Pd at the cross-sections of the **(a)** Pd(2.0)@IRA-900 and **(b)** Pd(2.0)@IRA-958 analyzed by EDS. The $R/R_0>0$ and $R/R_0<0$ (R: distance from the center, and R_0: radius of the resin bead) indicate scan positions along the radial coordinate as shown in Figure 2.

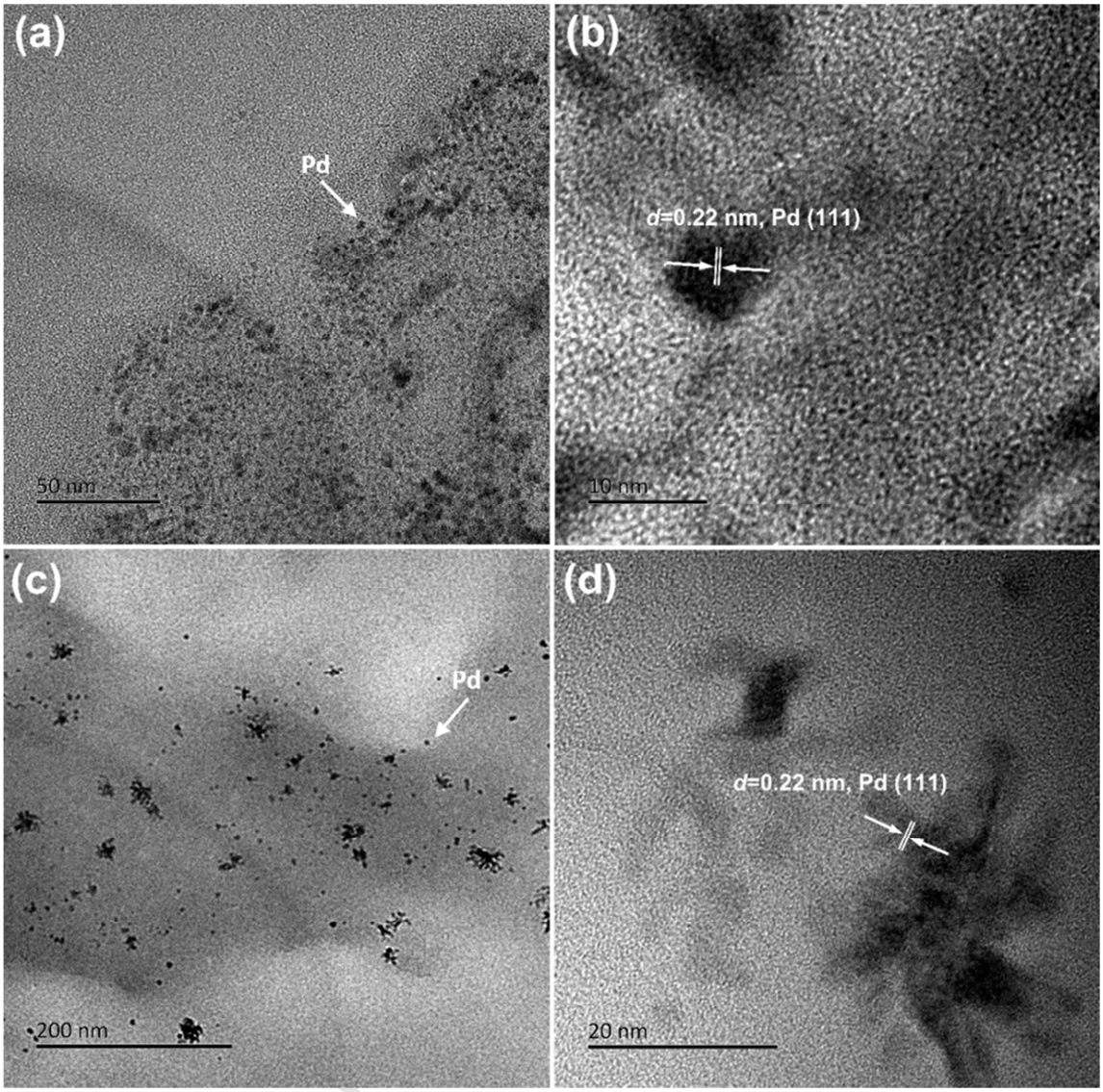

Figure 4. TEM and HRTEM images of Pd(2.0)@IRA-900 **(a and b)** and Pd(2.0)@IRA-958 **(c and d)**.

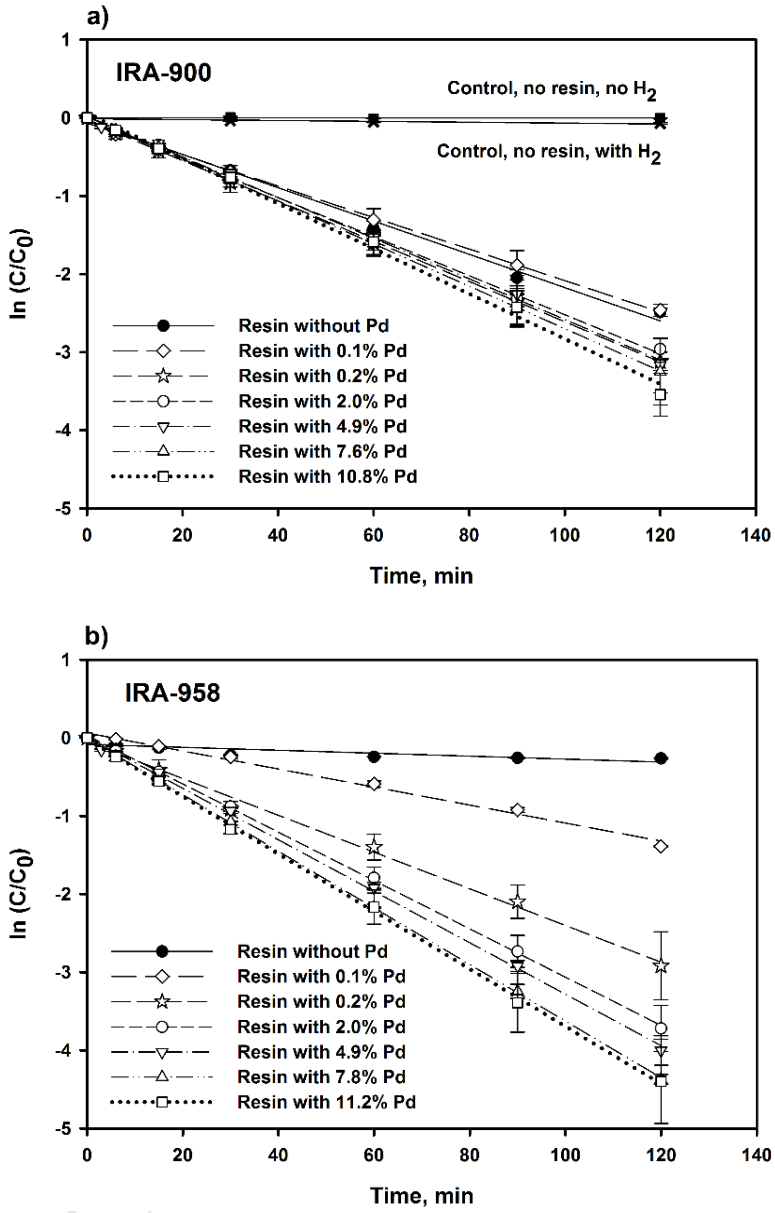

Figure 5. Linearized pseudo first-order kinetic profiles of catalytic hydrodechlorination of triclosan at different Pd loadings on resins **(a)** IRA-900 and **(b)** IRA-958. Initial [triclosan] = 2.9 mg/L, resin = 1 g/L, pH=4.9±0.2. Symbols: experimental data; Lines, pseudo first-order model fittings. Error bars are given as standard deviation.

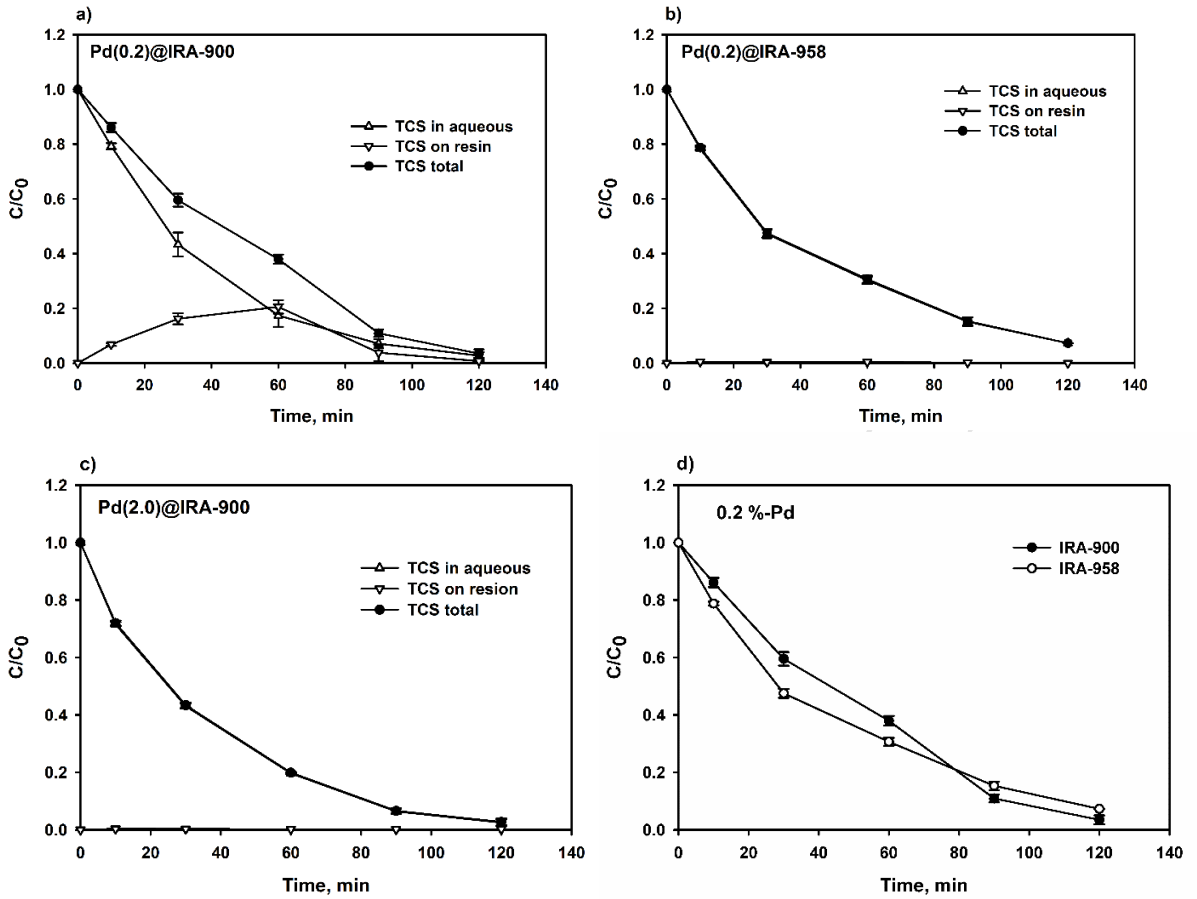

Figure 6. Degradation of adsorbed and dissolved triclosan in the course of catalytic hydrodechlorination with **(a)** Pd(0.2)@IRA-900, **(b)** Pd(0.2)@IRA-958, and **(c)** Pd(2.0)@IRA-900; and **(d)** comparison of solely hydrodechlorination of triclosan over two resin-supported catalysts. Initial [triclosan] = 2.9 mg/L, resin = 1 g/L, pH=4.9±0.2. Error bars are given as standard deviation.

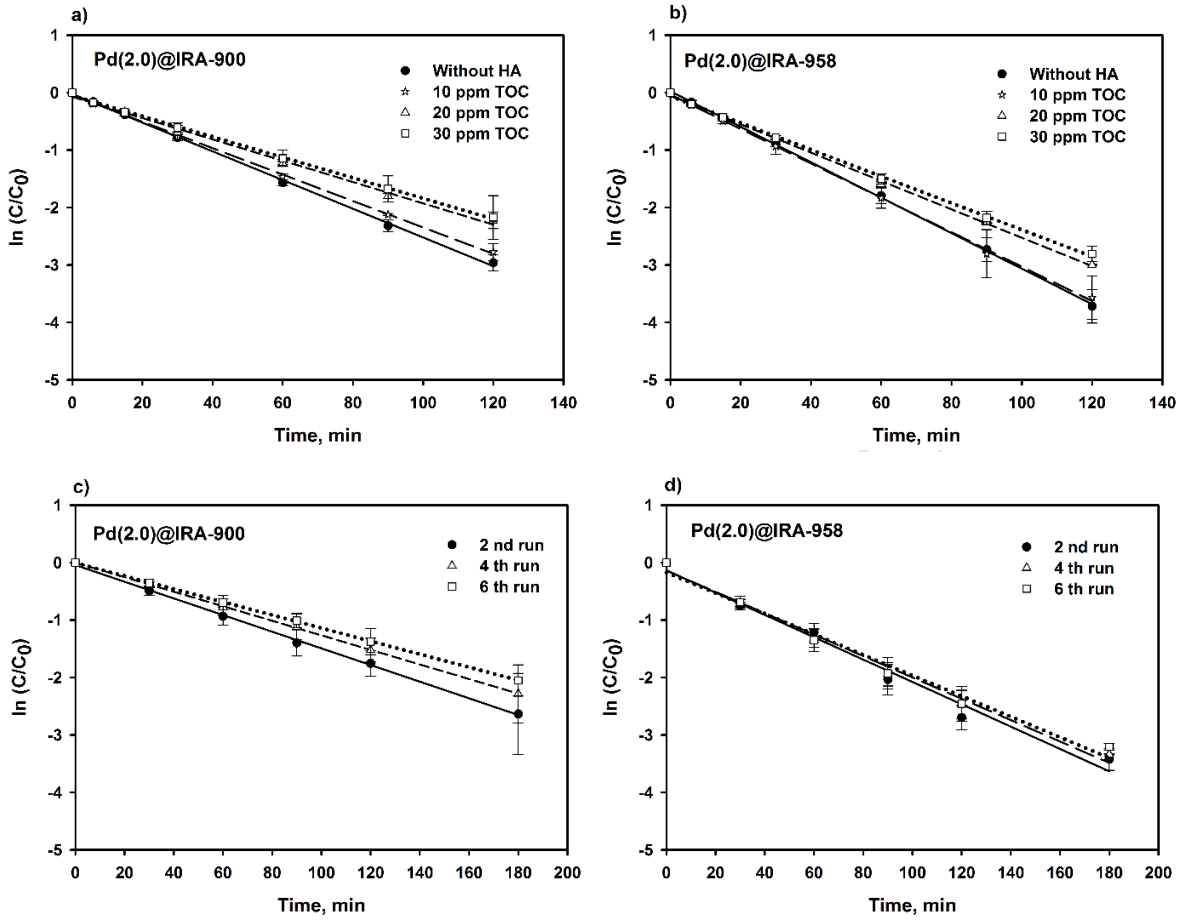

Figure 7. Linearized kinetic profiles of catalytic hydrodechlorination of triclosan by **(a)** Pd(2.0)@IRA-900 and **(b)** Pd(2.0)@IRA-958 in the presence of various concentrations of humic acid, and during Runs 2, 4 and 6 in six consecutive runs using **(c)** Pd(2.0)@IRA-900 and **(d)** Pd(2.0)@IRA-958 in presence of 30 mg/L HA as TOC. Initial [triclosan] = 2.9 mg/L, resin = 1 g/L. Error bars are given as standard deviation.

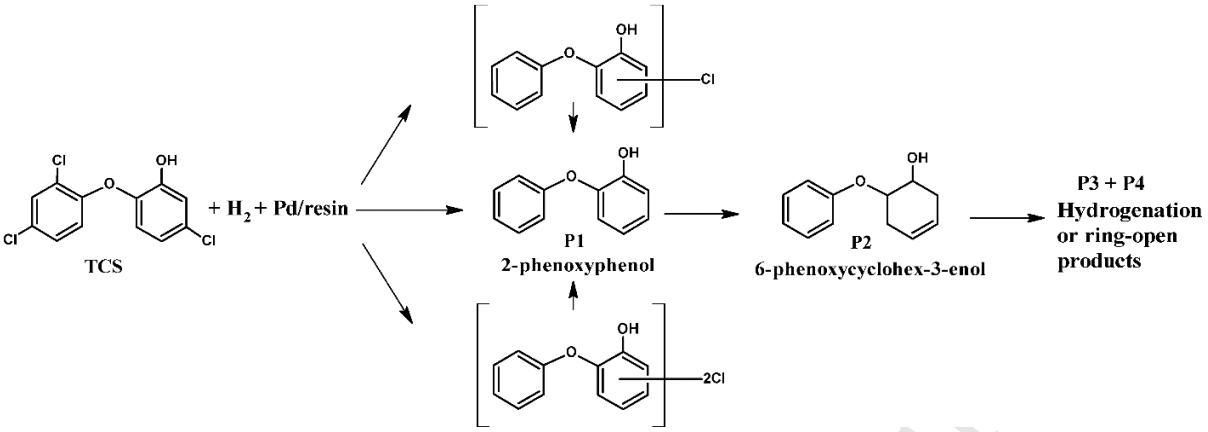

Figure 8. Reductive degradation pathway for catalytic hydrodechlorination of triclosan using resin-supported Pd catalysts.

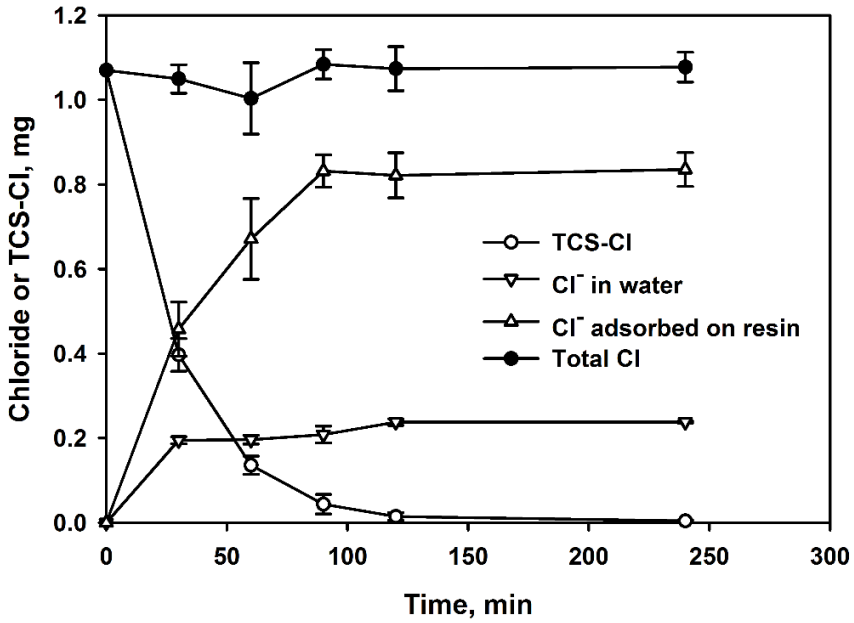

Figure 9. Concentration histories of Cl^- in the aqueous phase, Cl^- adsorbed on resins, and TCS-Cl (i.e., Cl in triclosan) during hydrodechlorination of triclosan using Pd(2.0)@IRA-958. Initial [triclosan] = 2.9 mg/L, resin = 1 g/L, pH=4.9±0.2. Error bars are given as standard deviation.

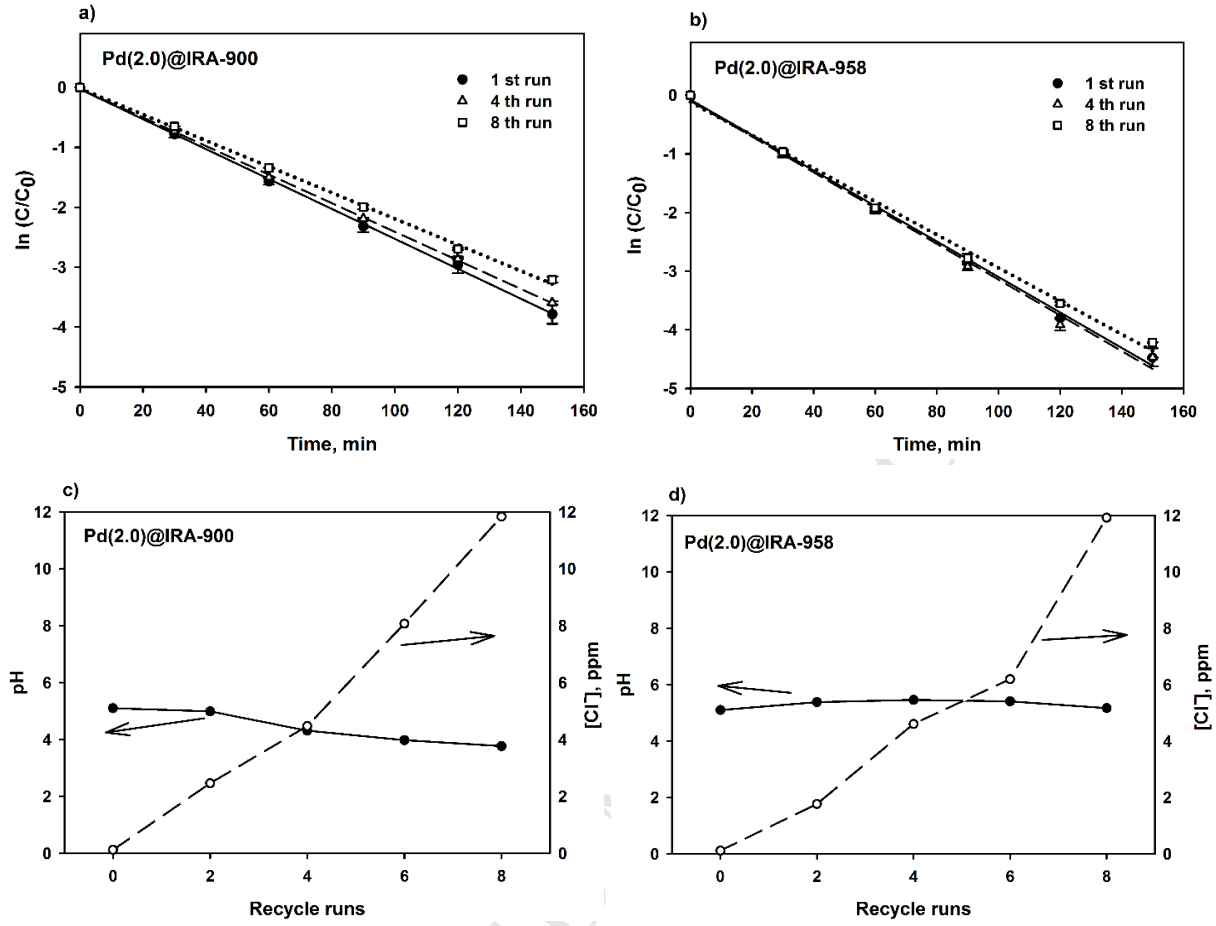

Figure 10. Linearized pseudo first-order plot of catalytic triclosan hydrodechlorination by **(a)** Pd(2.0)@IRA-900 and **(b)** Pd(2.0)@IRA-958 in Runs 1, 4 and 8 during eight consecutive runs; and histories of solution pH and [Cl^-] for **(c)** Pd(2.0)@IRA-900 and **(d)** Pd(2.0)@IRA-958. Initial [triclosan] = 2.9 mg/L, resin = 1 g/L. Error bars are given as standard deviation.

Highlights

- A new class of anion exchange resin supported palladium catalysts were prepared
- Initial uptake of Pd precursor anions facilitates controlled and uniform Pd loading
- Properties of resin matrices affect performance of the supported Pd catalysts
- The catalysts show high catalytic activity, great reusability and low Pd bleeding
- The catalysts are resistant to Cl^- poisoning and natural organic matter fouling